

Combined Probabilistic Methods for Droplet Drying Simulations

W. Wolak, A. Drzewiński, M. Marć, L. Najder-Kozdrowska, M.R. Dudek*

*University of Zielona Góra
Institute of Physics
ul. Szafrana 4a, 65-069 Zielona Góra, Poland
E-mail: m.dudek@if.uz.zgora.pl

Received: 15 November 2021; revised: 16 December 2021; accepted: 18 December 2021; published online: 29 December 2021

Abstract: The rapidly developing 3D printing and the related fabrication of ultra-thin layers in various industries have resulted in the need for theoretical methods for describing large-area systems of growing nanostructures. The specificity of these issues is the presence of multi-particle systems characterized by the coexistence of particles with a wide range of sizes typical for ions, nanoparticles, and their agglomerates. A particular example would be an aqueous nano-colloidal suspension drying on a substrate as a self-assembling deposit. It should be emphasized here that the development of deposit patterning control techniques is one of the most important challenges for the thin film industry. In this paper we show that probabilistic methods can be successfully used to model such systems. To this aim, the combined master equation and Monte Carlo methods were used for computer simulation of a drying droplet in the case of a low concentration salt solution. The novelty of this approach is to show the possibility of computer simulation for a microscopic system while simulating large-scale processes affecting microscopic processes. The numerical results were additionally supported by experimental data.

Key words: Monte Carlo, master equation, drying droplet, deposit patterning

I. INTRODUCTION

For this journal we are interested in computer simulation of the large-scale phenomena related to the drying of a droplet leading to the formation of a deposit on a substrate. It is known that such a deposit often takes the form of the coffee-ring structure which is undesirable for many industry applications. This phenomenon is well explained by Deegan and coworkers [1] but there is still a struggle to obtain deposit structures that are homogeneously distributed over the substrate without the presence of a coffee-ring structure [2–4]. When the edge of a drying drop is pinned to the substrate, the evaporation process leads to the appearance of capillary flow of droplet components (e.g. solute and colloidal particles) from the droplet center to its edge, causing the accumulation of particles at the droplet-substrate contact line. In this case, computer modeling of the deposit patterning requires overcoming both the barrier of direct access to

the huge computer memory and CPU requirements. An example of the application of the Monte Carlo method to simulate the droplet drying process can be found, among others, in the following publication [5] which presents the basic profiles of a drying droplet. The computational complexity of the problem is so great that the authors could only provide the coarse-grained results on the appearance of the coffee ring.

This study demonstrates the possibility of a hierarchical description of this issue in two stages. In stage I, the volume of the droplet's interior is divided into volumetric cells and the displacement of the solution components takes place through the probable flux flowing between adjacent volumetric cells. This is the exact enumeration method originating from the master equation approach. In stage II, the Monte Carlo method is exploited to simulate the deposit structure. To be specific, we choose a droplet of a low concentration salt solution as an example. The results are additionally sup-

ported by experimental data on imaging the drying droplet and deposit patterning using optical microscopy and atomic force microscopy (AFM).

II. MODEL

II. 1. Volumetric Simulation

In this work the physical system for a drying droplet is represented by a droplet of 0.02 M NaCl salt solution on a freshly cleaved mica surface. The mica surface is often said as the basic substrate for the atomic force microscopy (AFM) [6]. The atomically-flat surface of muscovite mica is a silicate layer structure where an octahedral layer of AlO_6 is located between every two tetrahedral layers of SiO_4 . In this structure, one in four Si^{4+} in the tetrahedral layers is randomly replaced by Al^{3+} thus generating a negative charge that is compensated by K^+ cations. During cleavage of the mica along the (001) crystal face, half of the potassium ions remain on each of the separated mica surfaces preserving charge neutrality. In the simulation program, the muscovite mica structure is approximated by a coarse-grained rectangular lattice with a unit cell with dimensions $a_x = 25$ nm and $a_y = 26.18$ nm, which makes the diagonal inclination in each cell equal to 60 degrees. This approximation of the mica surface partially reflects some features of the ditrigonal structure of the mica surface that was used in the experimental part concerning the drying saline droplet in Fig. 1 (see also Fig. 3).

The assumptions of the drying droplet model are the following:

1. We assume that the droplet surface $h = z(x, y)$ has a spherical cap shape with a circular solid-liquid cross-section with a radius R . The radius R does not change as the droplet dries. The droplet contact angle θ and

droplet height h decrease during the evaporation process according to the analytical equations for $\theta(t)$ and $h(t)$ [7, 8]. The detailed form of these equations is given below. During the computer simulation they determine the time-dependent boundary conditions for the diffusing ions Na^+ and Cl^- because water will not be directly included in the simulation. Moreover, the diffusing ions sense an outward drift due to the capillary flow caused by the water evaporation process and an inward drift due to the change in the shape of the droplet.

2. The droplet height $h = h(r, t)$ at distance r from its center is given analytically by the equation [8]

$$h(r, t) = \sqrt{R^2 / \sin^2(\theta) - r^2} - R / \tanh(\theta),$$

where $\theta = \theta(t)$ denotes the droplet contact angle at time t and $r^2 = x^2 + y^2$. According to the following paper [8]: $-\frac{dh}{dt} = D(1 - H)c_{\text{sat}}(0.27\theta^2 + 1.3)(1 + \cos(\theta))^2 / \rho R^2$.

The parameters used in the simulation run are vapor diffusivity $D = 26.1$ mm²/s, humidity $H = 0.38$, vapor saturation $c_{\text{sat}} = 2.32 \times 10^{-8}$ g/mm³, water density $\rho = 1$ g/cm³, and $R = 0.08$ mm.

3. The outward capillary flow velocity $u_{\text{outward}}(r)$ at distance r from the droplet center (Fig. 2) reads as the following: $u_{\text{out}} = D^* / (\theta \sqrt{R(R - r)})$ where $D^* = 2\sqrt{2}D(1.0 - H)c_{\text{sat}} / (\pi\rho)$.
4. The inward flow (Fig. 2) was defined with the help of the difference between the height at time $t + \Delta t$ and time t as follows:

$$u_{\text{inward}} = \alpha(h(t + \Delta t) - h(t)) / \Delta t$$

where $\alpha = z/h(t)$ and z is the z -component of the diffusing ion (Na^+ or Cl^-).

5. The inside of the droplet is partitioned into cube-shaped cells with a side length of 10 μm . In each cell there is a given number concentration of ions Na^+ and

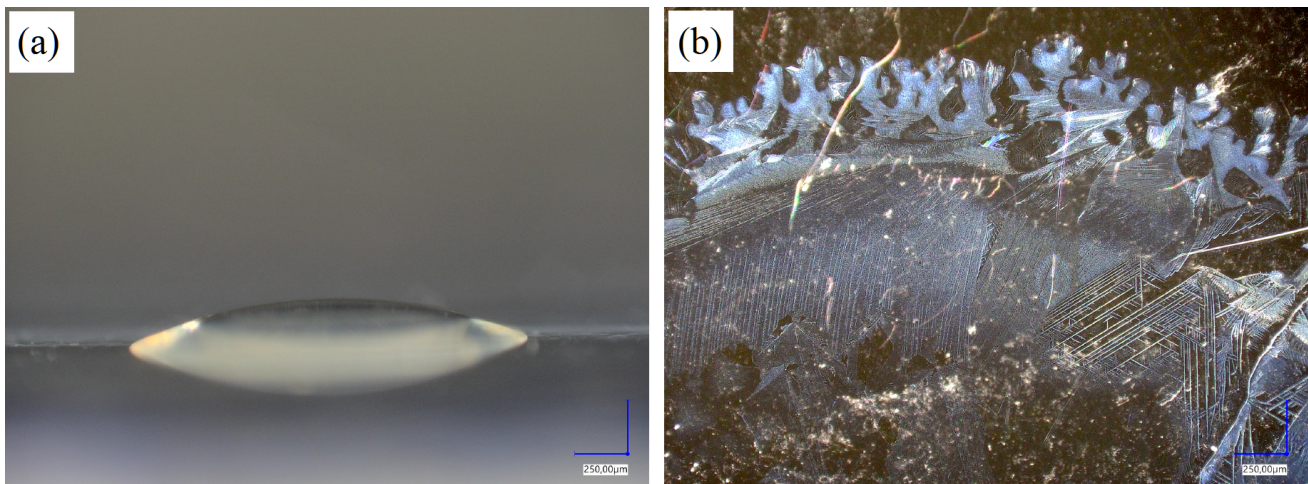


Fig. 1. Optical microscope image of a drying droplet of 0.02 M saline placed on the surface of muscovite mica (a), a fragment of the ring-like salt deposit representing the coffee ring structure

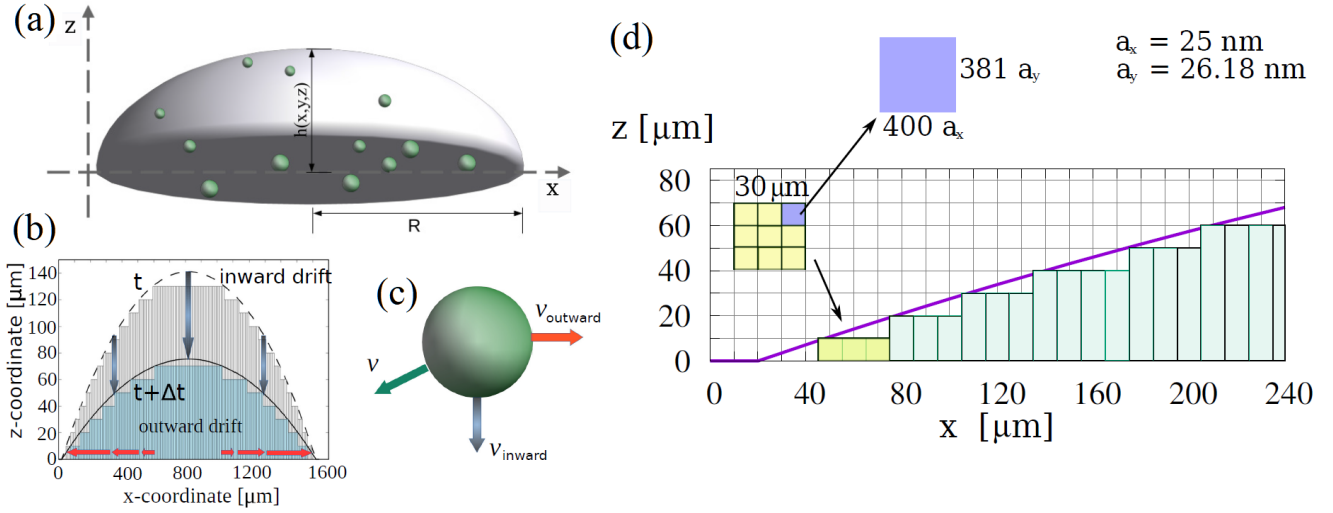


Fig. 2. Conceptual diagram of the drying droplet model that shows: (a) salt ions under the spherical cap of the droplet which is their diffusion limit, (b) the effect of decreasing the contact angle θ in the sequential time step and thus reducing the space for ion diffusion, (c) a single ion with arrows representing the velocities related to its diffusion and capillary flow to the outside and inside of the droplet, (d) an enlarged section of the space occupied by the droplet, where the area of nine cubes has been selected for modeling the deposit patterning in this fragment

Cl^- , which changes with time according to the calculated coefficients of the transition probability between neighboring cells as in the following master equation:

$$C(t+1)_{ijk} = \sum_{lmn} C(t)_{lmn} w_{lmn,ijk} - C(t)_{ijk} \sum_{lmn} w_{ijk,lmn}, \quad (1)$$

where (i,j,k) and (l,m,n) label the nearest neighbor volumetric cells and $w_{lmn,ijk}$ represents the probability transition rate from the cell (lmn) to the cell (ijk) , C_{ijk} denotes concentration of ions in the cell (ijk) . The rates w have the meaning of the inverse time τ ($w \sim 1/\tau$) it takes to move a single ion between adjacent cells. The values of τ are calculated with the help of the diffusional velocity of ions and the capillary flow velocities, u_{outward} and u_{inward} . It is assumed that the outward capillary flow characterized by the drift velocity u_{outward} takes place only in the cubes in the lowest layer. The inward flow induced by the drift velocity u_{inward} is sensed by ions in all cubes. The ions diffuse in the six natural directions w in a cubic unit.

- The part of the ion flux from the lowest cubic boxes directed to the substrate with a certain probability sticks to the substrate and the salt crystallines begin to grow. The probability of their growth is carried out according to the salt hopper growth model [9]. This type of salt crystal growth is suggested by our experimental section for a low concentration salt solution on a mica substrate. We observed a strong trend for the crystallines to grow dominantly along their edges analo-

gously to the hopper growth. In this case the supersaturation at the onset of crystallization in the solution is defined as $S_m = m_t/m_0$, where m_t and m_0 are the molal concentrations when the crystal precipitates at equilibrium [9]. We have selected the crystalline size L growth rate to be in accordance with the equation $dL/dt = K(S_m - 1)$, where $K = 9.4 \mu\text{m/s}$ and $S_m = 1$. It is worth adding that the number of nucleation points is a simulation parameter.

A schematic model of a drying droplet is shown in Fig. 2. Panel (a) presents the spherical cap of the droplet which is a boundary for diffusing ions. Ion diffusion takes place between the cubes inside the droplet. Each cube has an edge length of $10 \mu\text{m}$. Panel (b) shows the effect of decreasing the angle θ in the next time step, thus reducing the space for ion diffusion. Thereby, the concentration of ions in the cubes increases. A single ion is symbolically shown on panel (c), where the arrows represent the ion velocities related to its diffusion and capillary flow to the outside and inside of the droplet. Panel (d) shows an enlarged section of the space occupied by the droplet, where the area of nine cubes has been selected. The simulation of the salt crystallization will be carried in this area. The lowermost cubes contact the substrate which is represented by a rectangular mesh so that for each cube there is an area of $400a_x \times 381a_y$, where a_x and a_y represent the elementary cell of the substrate. In the case of $\theta = 0.1111$ and the radius $R = 0.8 \text{ mm}$, the droplet covers 153 206 cubes including the 20 060 cubes in the bottom layer in contact with the substrate. In the case of modeling the structure of the deposit, after determining the flow of salt ions towards the substrate, there is a need to simulate the

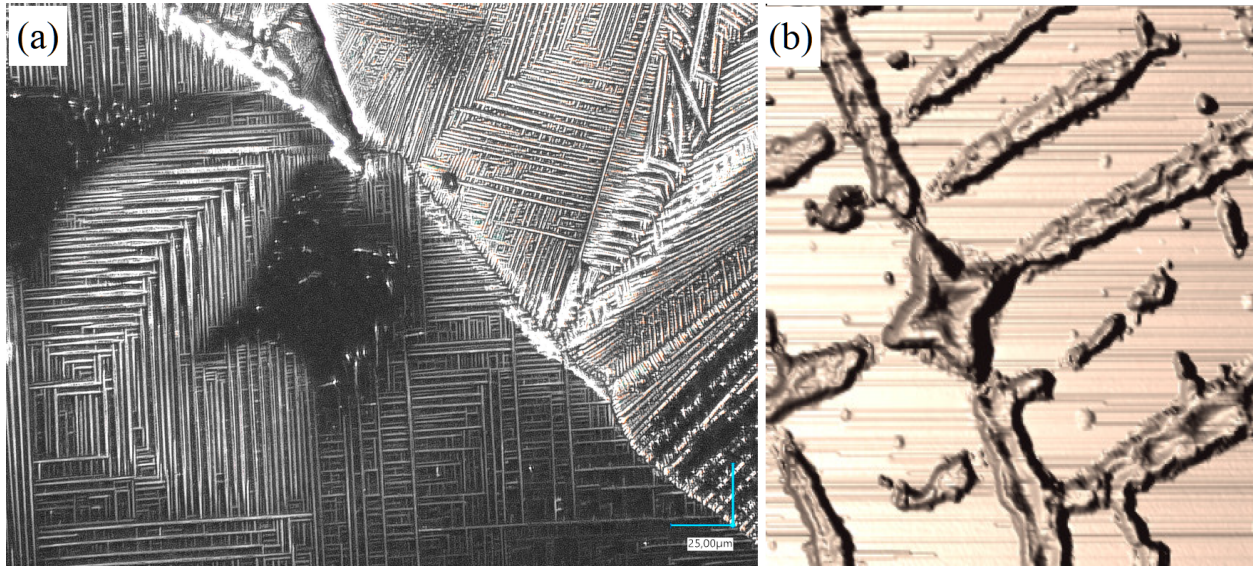


Fig. 3. Examples of elongated salt structures are shown: an optical microscope image (a), and 3D projection of an AFM image corresponding to the $15 \times 15 \mu\text{m}$ region with the hopper-like structure (b)

formation of a salt deposit on $N = 3\,057\,144\,000$ cells of a rectangular network representing the substrate. For this reason, in the model, the increase in the deposit is analyzed only on the part of the droplet corresponding to nine cubes arranged next to each other (see panel (d)) covering the area of $30 \times 30 \mu\text{m}$. In the remaining cubes the total concentrations of the crystallized salt are saved without performing a patterning process. In this way, it is possible to model the deposit patterning only in the selected places. Evidently, this is a large approximation because this cut-off procedure excludes the presence of deposit aggregates that could appear from the outside areas. In this work, 9 contiguous areas were selected for the presentation of the applied computer simulation method. The number of them and their location on the substrate can, however, be increased freely, allowing an insight into the crystallization processes taking place in them. This is a significant strength of the method because it shows the possibility of computer simulation of a large-area phenomenon while ensuring its impact on processes on a microscopic scale in selected locations. The size of the simulation box in these selected areas will depend only on the characteristic wavelength of the considered physical phenomenon.

II. 2. Deposit Patterning Simulation

In the simulations the area selected for the modeling of the deposit patterning relates to 9 adjacent faces of the cubes contacting the substrate and thus it means a 3600×3429 mesh made of cells with sides a_x, a_y . This area overlaps a fragment of the coffee ring structure of the deposit as it is shown in Fig. 2. To optimize the access to the computer's memory, this area was divided into 9 square areas, with the linear size of $10 \mu\text{m}$, corresponding to the cube faces. Consequently, the simulation of the deposit growth was carried out

in 9 areas representing a grid with 400×381 lattice sites. The information about the event that the salt crystal grows outside its area towards the adjacent one is a cause for updating the deposit on the adjacent lattice. The crystalline growth outward the 9×9 area is forbidden.

In the case of a low concentration salt solution, the pattern formation in our model represents a two-dimensional aggregation problem on the rectangular lattice. The effect of surface tension for the growing deposit is included with the help of the sticking probability that depends on the local curvature κ of the deposit. We adopted the method of modeling the pattern formation that was introduced by Vicsek [10]. Then the sticking probability is the following:

$$p(\kappa) = A\kappa + B, \quad (2)$$

where

$$\kappa = m/L_2^2 - (L_2 - 1)/(2L_2), \quad (3)$$

and L denotes the range expressed in lattice sites that is used for the 2D surface curvature calculation, m denotes the number of the lattice sites within this range which have been covered by the deposit. In Eq. (3), $L_2 = 2L$. The Metropolis Monte Carlo is used for the sticking events. To model the deposit formation initially some number of the nucleation sites is selected at random. The new crystallines can overlap the existing ones but the distance between their centers cannot exceed a given value.

III. RESULTS AND DISCUSSION

The theoretical results of the large-area simulations of the drying droplet problem were supported by the experi-

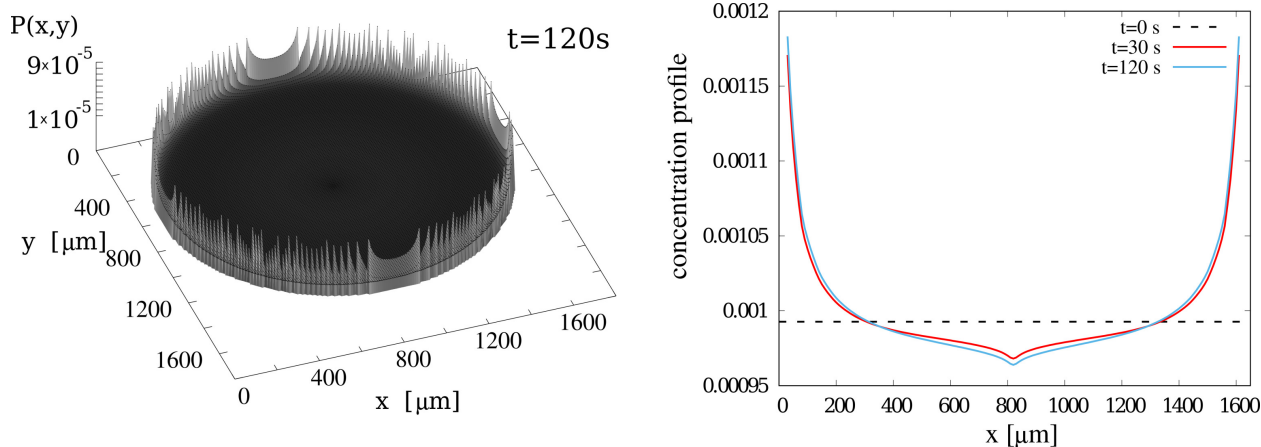


Fig. 4. The ring-like structure of the droplet deposit after 120 s (a), and the net number concentration profiles of salt ions in cubes representing the section of the droplet along the x -direction at different times (b)

mental results for a drying droplet of 0.02 M NaCl salt solution. Fig. 1a shows the image under the optical microscope for a droplet placed on the freshly cleaved muscovite mica. In the next figure (Fig. 1b), a fragment of the droplet deposit is shown together with a fragment of the coffee-ring structure. In this area there are evident characteristic longitudinal nanostructures which are typical for the salt solutions of very low concentration. They range in thickness from a few nanometers to several hundred. These structures are also shown in Fig. 3. At the initial stage of the drying process their growth is not volumetric. Instead, the salt crystals mainly grow at their edges. This makes them very similar to the hopper structures [9]. In the right panel in Fig. 3, which shows the AFM image of a small fragment of the salt nanowires, an inverse pyramid structure characteristic for the hopper growth can be noticed. The thickness of the nanocrystalline chains is about 200 nm.

To perform a computer simulation of the drying droplet up, along with modeling of the deposit pattern, physical phenomena should be taken into account on several scales simultaneously, ranging from ion diffusion to macroscopic capillary flows in the droplet. These flows determine the macroscopic structure of the deposit. Presently, we have shown that computational difficulties can be relatively easily overcome by using combined probabilistic methods. In our case it is the master equation method for modeling ionic fluxes in the volume of the droplet and the Monte Carlo method for deposit patterning which can be restricted to a small fragment of the substrate. In the case of the small area of the substrate, such as in this study, the computational difficulties are reduced to the computing power of PC-level computers. In Fig. 4a, the coffee-ring structure for a drying droplet is shown in terms of the probability density represented by the number concentration of ions Na^+ and Cl^- per cube volume ($10 \mu\text{m}^3$). In Fig. 4b, the profile of the net concentration of both types of ions has been shown at different

times through the section of the drying droplet. It includes both the solution ions and the ions in the salt deposit, where the dashed line marks their initial distribution. In this study the simulation applies only to the initial stage of the drying droplet because the thin layer droplets of the low concentration salt solutions can undergo rupture that can strongly affect the deposit patterning. The issue is described in [11], but this mechanism is not included in our model.

The results of the computer simulation of the deposit pattern on the substrate are shown in Fig. 5 for the selected $30 \times 30 \mu\text{m}$ area at the edge of the droplet. The figure demonstrates a significant difference in the concentration and size of the salt structures in the individual nine sub-areas indicated by the dashed lines. These sub-areas correspond to the sizes of the lower face of the cubes representing the interior of the droplet, and the visible abrupt differences in the vertical direction are related to the simulation of ion flows between the cubes. The size of the cubes determines the resolution of the ionic flux to the substrate. This is also the reason for the more uniform concentration of the deposit in the horizontal direction. The resolution of the flux transfer is a parameter of our model, so the linear size of the cubes can be reduced. However, the figure correctly reproduces the structure of the deposit in the form of elongated nanostructures characteristic of hopper growth. The lower three regions are the outermost regions of the droplet and the size of these structures is much larger than those deeper into the droplet. Among others, they mimic well the fragment of the coffee ring structure. The right panel shows the analogous results for the smaller droplet with the radius $R = 0.6 \text{ mm}$. The division of the selected area into separate nine sub-areas did not introduce correlations once the deposit structures grow through their edges. The reason is that sticking probability is based on the local curvature of the deposit (Eq. (3)). In addition, even the clouds of the small salt structures are correlated accordingly.

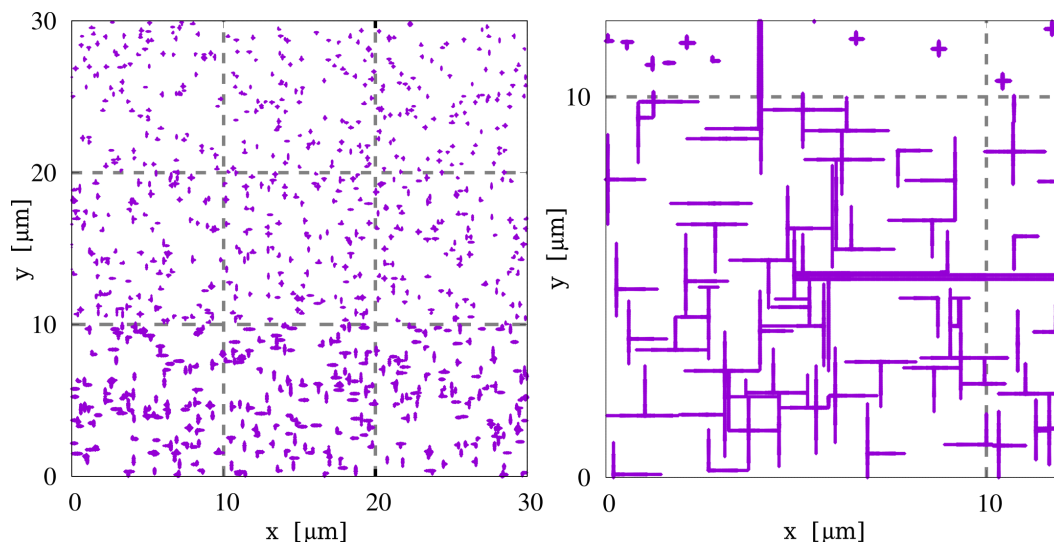


Fig. 5. The salt nanostructures emerge after the 120 s of the computer simulation of the drying droplet. In the left panel, the fragment of 9×9 square-like areas which are separated by the dashed lines is shown where the bottom squares represent the droplet edge. In this case $R = 0.8$ mm. In the right panel, the enlarged fragment of the deposit is shown for a droplet with $R = 0.6$ mm. Other parameters: $A = 3$, $B = 0.2$, $L = 11$ in $p(\kappa)$ (Eq. (2))

IV. CONCLUSIONS

Our results show that we were able to perform large-area simulations of the complex system like droplet deposit patterning. The combined probabilistic method based on the exact enumeration through the master equation approach and the Metropolis Monte Carlo method appears to be a promising approach for modeling complex systems. A specific example of the saline droplet can be easily extended to nanocolloidal droplets. The latter case is important to support experiments in which thin layers are built.

Acknowledgment

This research was funded by the Polish Ministry of Science and Higher Education under the program “Regional Initiative of Excellence” in 2019–2022, project No. 003/RID/2018/19, funding amount PLN 11 936 596.10.

References

- [1] R.D. Deegan, O. Bakajin, T.F. Dupont, G. Huber, S.R. Nagel, T.A. Witten, *Capillary flow as the cause of ring stains from dried liquid drops*, *Nature* **389**, 827–829 (1997).
- [2] R.G. Larson, *Re-Shaping the Coffee Ring*, *Angew. Chem. Int. Ed.* **51**, 2546–2548 (2012).
- [3] P.J. Yunker, T. Still, M.A. Lohr, A.G. Yodh, *Suppression of the coffee-ring effect by shape-dependent capillary interactions*, *Nature* **476**, 308–311 (2011).
- [4] D. Soltman, V. Subramanian, *Inkjet-Printed Line Morphologies and Temperature Control of the Coffee Ring Effect*, *Langmuir* **24**, 2224–2231 (2008).
- [5] A. Crivoi, F. Duan, *Three-dimensional Monte Carlo model of the coffee-ring effect in evaporating colloidal droplets*, *Sci. Rep.* **4**, 4310 (2014).
- [6] H.K. Christenson, N.H. Thomson, *The nature of the air-cleaved mica surface*, *Surf. Sci. Rep.* **71**, 367–390 (2016).
- [7] H. Hu, R.G. Larson, *Evaporation of a Sessile Droplet on a Substrate*, *J. Phys. Chem. B* **106**, 1334–1344 (2002).
- [8] H. Okada, S.N. Atluri, *Computational and Experimental Simulations in Engineering*, *Mechanisms and Machine Science* **75** (2020).
- [9] J. Desarnaud, H. Derluyn, J. Carmeliet, D. Bonn, N. Shahidzadeh, *Hopper Growth of Salt Crystals*, *J. Phys. Chem. Lett.* **9**, 2961–2966 (2018).
- [10] T. Vicsek, *Fractal growth phenomena*, World Scientific Publishing Co. Pte. Ltd. (1992).
- [11] G.F. Harrington, J.M. Campbell, H.K. Christenson, *Crystal Patterns Created by Rupture of a Thin Film*, *Cryst. Growth Des.* **13**, 5062–5067 (2013).



Wiktor Wolak obtained his doctoral degree in Physics from the University of Zielona Góra in 2019. He is currently working at the Institute of Physics, University of Zielona Góra. He has participated in several research projects related to nanostructure physics. His current interests include nanoparticle physics. He has experience in working with atomic force microscope, optical microscope, Raman spectroscope, 3D printers using fused deposition and stereolithography modeling, Monte-Carlo simulation method.



Andrzej Drzewiński was born in 1959 and is Professor at the Institute of Physics of the University of Zielona Góra (UZ) and Dean of the Faculty of Physics and Astronomy. He is a physicist specializing in methods of statistical physics. His topics of interest are phase transitions and critical phenomena, dynamics of polymers, molecular magnetism, and functional materials.



Maciej Maré has received his master's degree (Physics) from the University of Wrocław in 2010 and his doctoral degree (Physics) from the University of Zielona Góra in 2019. Currently he is employed as an assistant professor at the Institute of Physics, University of Zielona Góra. His major area of interest is the application of novel, nanostructured materials based on iron oxides, silica and titanium dioxide to industry and biomedicine.



Lidia Najder-Kozdrowska graduated in Physics from the Pedagogical University in Zielona Góra in 2001. She has been working at the Institute of Physics in Zielona Góra since 2001 and received the doctoral degree from the University of Zielona Góra in 2006. She was a scholarship holder of the German Research Foundation at the Institute of Biophysics of the Saarland University (Homburg / Saar) in 2006. Her research interest is focused on electron paramagnetic resonance of coal, melanin, zeolites and medical physics.



Mirosław Roman Dudek was born in 1956. He is employed as Professor at the University of Zielona Góra. His main field of interest is nanotechnology: experiment and theory. He has experience in the methods of statistical physics, computer modeling, issues of genetic evolution, and methods of DNA analysis.